

Photon assisted tunneling of high order multiple Andreev reflections in epitaxial nanowire Josephson junctions

Damon James Carrad,^{*,†,‡,§} Lukas Stampfer,^{†,§} Dāgs Olšteins,[†] Christian
Emmanuel Noes Petersen,[†] Sabbir A. Khan,^{†,¶} Peter Krogstrup,[†] and Thomas
Sand Jespersen^{*,†,‡}

[†]*Center for Quantum Devices, Niels Bohr Institute, University of Copenhagen, 2100
Copenhagen, Denmark*

[‡]*Department of Energy Conversion and Storage, Technical University of Denmark,
Fysikvej, Building 310, 2800 Kgs. Lyngby*

[¶]*Danish National Metrology Institute, Kogle Alle 5, 2970 Hørsholm, Denmark*

[§]*These two authors contributed equally*

E-mail: damonc@dtu.dk; tsaje@dtu.dk

Abstract

Semiconductor/superconductor hybrids exhibit a range of phenomena that can be exploited for the study of novel physics and the development of new technologies. Understanding the origin the energy spectrum of such hybrids is therefore a crucial goal. Here, we study Josephson junctions defined by shadow epitaxy on InAsSb/Al nanowires. The devices exhibit gate-tunable supercurrents at low temperatures and multiple Andreev reflections (MARs) at finite voltage bias. Under microwave irradiation, photon assisted tunneling (PAT) of MARs produces characteristic oscillating

sidebands at quantized energies, which depend on MAR order, n , in agreement with a recently suggested modification of the classical Tien-Gordon equation. The scaling of the quantized energy spacings with microwave frequency provides independent confirmation of the effective charge ne transferred by the n^{th} order tunnel process. The measurements suggest PAT as a powerful method for assigning the origin of low energy spectral features in hybrid Josephson devices.

Keywords: semiconductor/superconductor hybrids, nanowires, multiple Andreev reflections, photon assisted tunneling, Tien-Gordon

Traditional Josephson junctions (JJ)¹ – where two superconductors are coupled through a thin tunnel barrier – constitute the most important device element in superconducting electronics and in state-of-the-art superconducting quantum information processors.² Recently, there has been an increasing interest in merging the quantum properties of superconductors with the electrostatic control of semiconductor electronics. For example, semiconductor-based JJs allow electrostatic tunability of the Josephson coupling,³ enabling gate-tunable superconducting qubits,⁴ and qubit implementations based on the Andreev bound states of few-channel JJs⁵ or topologically protected low-energy states in one-dimensional proximity-coupled semiconductor/superconductor hybrid devices.^{6,7} In all cases, the electronic states in semiconductor/superconductor hybrid materials are of fundamental importance. The spectrum can be probed using normal/superconductor spectroscopy,^{8–10} microwave spectroscopy¹¹ or by measuring finite-bias transport in semiconductor JJs.¹² In the latter case, however, low energy spectral features can both be related to states of the leads or to higher order transport processes.^{13–16} Sharp spectral features are expected to appear at voltages $\pm 2\Delta/ne$ due to the sequential opening and closing of the allowed orders $n = 1, 2, \dots$ of multiple Andreev reflection (MAR) processes. The MAR energies are independent of the junction transparency and analysis of the sub-gap spectrum allows extraction of the superconducting gap^{12,17} and the determination of channel transmission of the junction.^{18,19} In nanoscale semiconductor JJs, unambiguous assignment of MAR features in transport be-

comes problematic due to potential modifications of the sub-gap spectrum including from charging phenomena^{20–22} and intrinsic properties of the semiconductor such as spin-orbit coupling.^{23,24} This is increasingly important for processes of higher-orders – i.e. lower energy – where strong peaks unrelated to MAR can appear in the tunnel spectrum,²⁵ heating effects may modify the gap and thus the MAR positions, and MAR orders have been observed to be missing from the spectrum for reasons not yet understood.²⁶ Looking beyond the hybrid device studied in this manuscript, understanding of sub-gap spectra is crucial for interpreting results from the powerful tool of superconducting scanning tunneling microscopy,²⁷ which allows special mapping of sub-gap states and is applicable to a wide variety of materials.

A characteristic feature which could distinguish MAR processes and their orders is the transferred charge: The n^{th} -order process, dominating at $V_{sd} = 2\Delta/ne$, transfers a charge $q_n = ne$ across the junction.²⁸ While the sub-gap spectrum has been extensively investigated,^{13–16} only a few studies have directly addressed q_n . In Refs.^{29–31} q_n was investigated through the bias scaling of the noise spectrum of JJ which was found to be consistent with the prediction. Recently, an alternative method for measuring q_n has been suggested based on the evolution of the sub-gap spectrum under microwave irradiation.^{27,32,33} Due to the Tien-Gordon effect^{34,35} – or photon assisted tunneling (PAT) – modulating sidebands are expected in the non-linear sub-gap spectrum around the n^{th} MAR structure. While the conventional Tien-Gordon model predicts a characteristic modulation scale of $\delta V = \hbar f/e$ where f is the frequency of the microwave field, Ref.^{32,33} suggested that in higher order processes the total transferred charge should be used. This was consistent with measurement of quasi-particle tunneling ($1e$) and incoherent Cooper pair tunneling ($2e$), and is consistent with early studies of the sub-gap spectrum at fixed microwave frequency and power.¹¹ In this letter we present measurements at varying microwave power and frequency of PAT of the sub-gap spectrum in epitaxial semiconductor/superconductor InAsSb/Al nanowire JJs realized by shadow lithography.^{36,37} The measurements show clear signatures of the charge $q_n = ne$ of the n^{th} order MAR up to $n = 3$.

InAsSb nanowires (NWs) were grown by molecular beam epitaxy following the procedure of Ref.³⁶ Parallel trenches were etched in a (100) InAs substrate and 90 – 120 nm diameter NWs were grown from Au catalyst particles positioned on opposing (111)B inclined side facets. As shown in Fig. 1a, the growth position of the NWs were laterally offset such that neighboring NWs defined ~ 100 nm wide shadow gaps^{38,39} in the 15 nm thick, epitaxially matched Al film (arrow).^{36,37,40,41} NWs were transferred to a doped silicon substrate capped with 100 nm SiO₂, and contacts to the Al half-shell were defined using established lithographic methods.^{36,37,40,42} Figure 1b shows a SEM micrograph of a typical finished device and schematic measurement circuit. The conducting Si substrate acted as back-gate, which was used to alter the carrier density in the exposed InAsSb. Each contact electrode was split into two individual bond pads to facilitate pseudo-four terminal measurements of the device resistance, eliminating series resistances from e.g. low pass filters in the cryostat cabling. The remaining series resistance – likely dominated by the contacts – ~ 3 k Ω , was identified as a constant off-set in the supercurrent regime and was subtracted in the following. Measurements were performed in a dilution refrigerator with a base temperature of 15 mK and microwave radiation was coupled to the device by a coaxial line with ~ 12 mm of the inner conductor left exposed and situated ~ 5 mm above the sample.

Figure 1c shows the differential resistance, dV/dI , as a function of current through the device, I , and back-gate voltage V_G . A zero resistance supercurrent is observed for low $|I|$. The current was swept from positive to negative (arrow) and the switching(re-trapping) current where the device transitions to(from) a resistive state from(to) the superconducting state is indicated. The differences in I_{sw} and I_r are commonly observed in nanowire JJs³ and ascribed to a consequence of Joule heating in the dissipative regime and/or underdamped dynamics of the JJ.^{43,44} Both I_{sw} and I_r decrease upon lowering V_G as expected from a JJ with constant $I_c R_N = \pi\Delta/2e$ and an n -type semiconductor which depletes with lowering V_G . Here I_c is the critical current and R_N is the normal-state device resistance. The aperiodic oscillations in $I_{sw}(V_G)$ appearing in addition to the overall gate-dependence

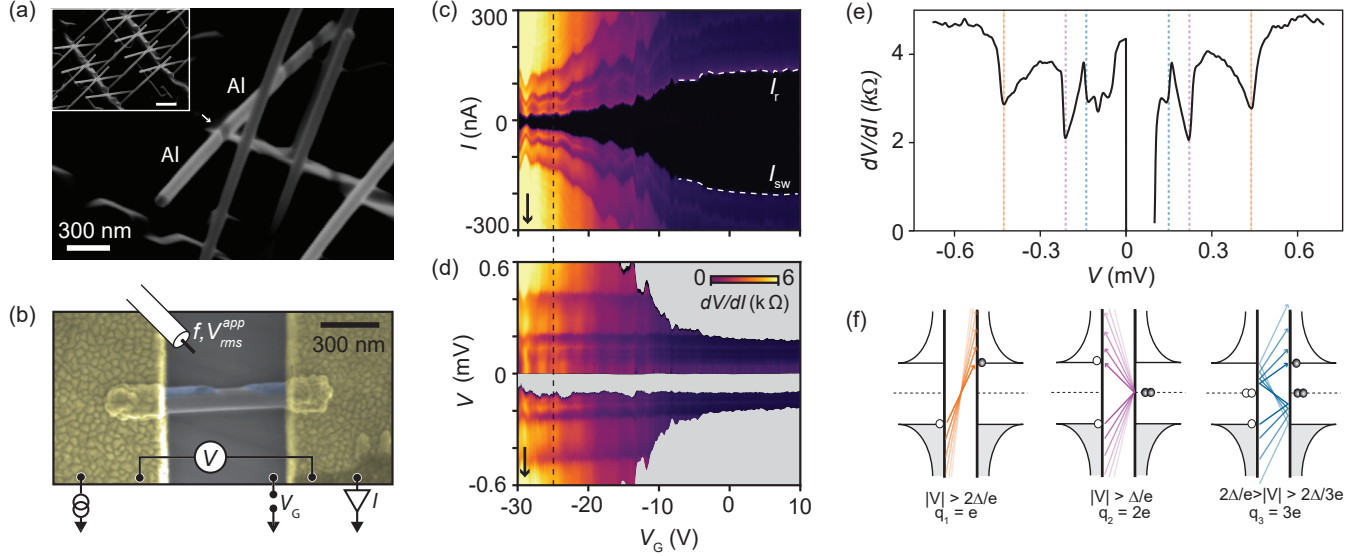


Figure 1: (a) Scanning electron micrograph (SEM) of as-grown InAsSb/Al nanowires. Al deposition was performed from roughly bottom-right to top-left across the image, and forward-positioned nanowires shadow those behind resulting in Al gaps (arrow). Scale bar in inset is 1 μm . (b) False colour SEM of a device featuring InAsSb nanowire (grey), shadow-patterned Al layer (blue) and Ti/Au ohmic contacts (gold). (c,d) Gate dependence at $T = 15\text{ mK}$ of the differential resistance dV/dI vs. measured current I , and voltage V , respectively. A zero resistance supercurrent is present between switching and retrapping currents I_{sw} , I_r . (e) Line trace in (d) at fixed $V_G = -25\text{ V}$. Dashed lines indicate features at voltages $\pm 2\Delta/e$ (orange), $\pm \Delta/e$ (purple), and $\pm 2\Delta/3e$ (blue) with $\delta = 225\text{ }\mu\text{eV}$ attributed to $n = 1, 2, 3$ MAR. The corresponding transport processes are schematically illustrated in (f).

is attributed to universal conductance fluctuations in $R_N(V_G)$.³ At $V_G \sim -25\text{ V}$ the normal state resistance is $R_N \sim 4.5\text{ k}\Omega$ and $I_{\text{sw}}R_N = 200\text{ }\mu\text{V}$, relatively close to the theoretical value $\pi\Delta_{\text{Al}}/(2e) = 350\text{ }\mu\text{V}$, as previously reported for similar hybrids.³⁶ The measured excess current (Supporting Fig. S1) $I_{\text{ex}} \sim 50\text{ nA}$ corresponds to a junction transmission of ~ 0.7 .⁴⁵

For I above/below the zero-resistance region in Fig. 1c, dV/dI exhibits a rich structure which follows the trend of I_{sw} and I_r . To gain insight into the origin of these features, Fig. 1d shows the same data as a function of the measured voltage V . Upon sweeping I down from zero, the voltage remains $V = 0\text{ V}$ until it abruptly switches at I_{sw} to a finite value. Therefore no data is obtained with V below this value, and this region is greyed-out in Fig. 1d. Conversely, V gradually decreases to zero around I_r when sweeping I down from positive values due to the underdamped junction dynamics,^{43,44} enabling data extraction

down to $V = 0$ for $I > 0$. As expected for MAR, the structure in Fig. 1d appears at fixed voltages despite the variation in conductance with V_G . Figure 1e shows a line trace of dV/dI vs. V for fixed $V_G = -25$ V. The three most pronounced dips are highlighted by dashed lines and follow $\pm 2\Delta/e$ (orange), $\pm\Delta/e$ (purple), and $\pm 2\Delta/3e$ (blue) with $\Delta = 225 \mu\text{eV}$ consistent with prior results from 15 nm thick Al.^{36,42,46} This series is expected for MAR and the relevant processes transfer charges of $1e$, $2e$ and $3e$ and are illustrated in Fig. 1f, where the slopes of the arrows represent voltage biases. Direct quasi particle tunneling ($1e$) occurs for $|V| \geq 2\Delta/e$. In the general case of $n \geq 2$, the n^{th} order process involves $n - 1$ Andreev reflections, a charge transfer of ne , and is allowed for $|V| \geq 2\Delta/(ne)$. Suppression of $n \geq 3$ processes occur for $e|V| \geq 2\Delta/(n - 2)$ due to the low probability of Andreev reflection above the gap.⁴⁷ Overall, the dc transport characteristics in Fig. 1 are comparable to previous NW-based JJs.^{3,25,26,48}

We now consider the features arising from irradiating the device with microwaves. Figure 2a shows dV/dI vs. V and the rms amplitude, $V_{\text{app}}^{\text{rms}}$, of 6 GHz microwave radiation, as applied to the antenna (Fig. 1b). The gate voltage was fixed at $V_G = -25$ V as in Fig. 1e – similar features were observed at other V_G , see Supporting Section II – and I was swept from negative to positive. A series of ‘V’-shaped patterns are observed, fanning out from $V_{\text{app}}^{\text{rms}} = 0$. The structure emerging from $V = 0$ V – i.e., when the JJ carries a supercurrent – is due to Shapiro steps^{1,49} caused by phase-locking between the microwave field and the superconducting phase difference across the JJ leading to a step-wise increase of V in units of $hf/(2e)$. In Supporting Fig. S3, we replot this regime as a function I as is common for studies of Shapiro steps, showing the conventional Shapiro pattern.^{3,48,50,51} The measurements are well-described by the extended RCSJ model and will not be considered further here.

The remaining V-shaped structures in Fig. 2a, which evolve from the MAR features at finite V , have a different origin and are the main focus of this work. Since the junction does not carry a supercurrent, phase locking and the resultant Shapiro steps do not occur. Instead, we attribute the structures to photon assisted tunneling. In general, for any two

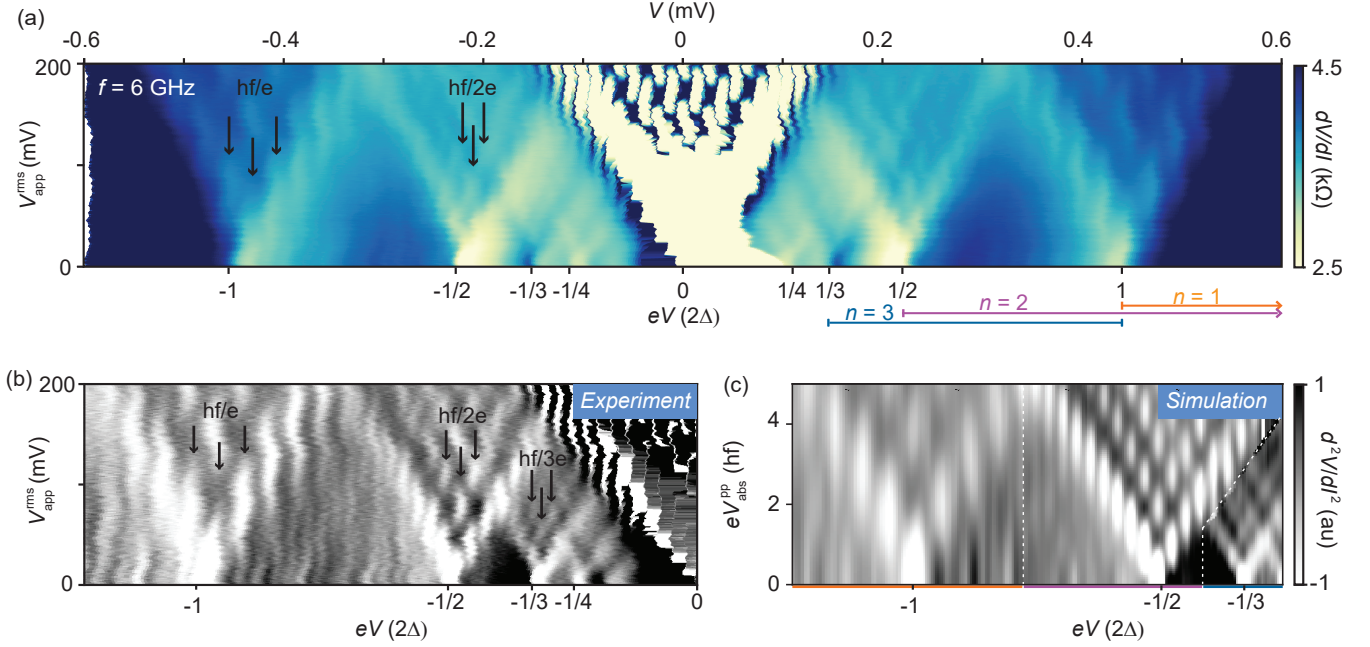


Figure 2: (a) Differential resistance at $V_G = -25\text{V}$ as a function of bias, V , and the rms amplitude of 6 GHz microwave radiation. The bottom axis represents energy E in units of 2Δ , with $\Delta = 225 \mu\text{eV}$ and the energy intervals for the first three MAR processes are indicated by horizontal lines. (b) The second derivative, d^2V/dI^2 , in a region of (a) around the higher order MAR showing the Tien-Gordon modulation in the $n = 2$ and $n = 3$ MAR processes. The changing period of modulation is indicated by arrows. (c) A simulation of the data in (b), based on Eq. 1 modified to account for the charge of the higher order transport processes. Processes of different order are assumed to dominate in the indicated regions.

terminal device absorbing radiation at frequency f , charges can absorb/emit photons and thereby gain energy $\pm hf$ and tunnel across the junction – here h is the Planck constant and $l = 0, \pm 1, \pm 2, \dots$. Thus, at finite irradiation amplitude, the current at the dc voltage V is related to the dc current in the absence of irradiation, I^0 , at $V \pm hfl/e$. For smooth $I^0(V)$, this has no consequence, however, non-linearities in $I^0(V)$ will repeat at finite radiation amplitude as sidebands with an intensity modulated by the radiation amplitude. In the simplest case where the radiation field on the sample is sinusoidal, $V_{\text{abs}} = V_{\text{abs}}^{\text{pp}} \cdot \sin(2\pi ft)$, the current at finite radiation amplitude is given by the Tien-Gordon equation:³⁴

$$I_{\text{dc}}(V) = \sum_l J_l^2 \left(\frac{eV_{\text{abs}}^{\text{pp}}}{hf} \right) \cdot I^0 \left(V + \frac{hfl}{e} \right) \quad (1)$$

where $J_l(x)$ is the l^{th} Bessel function. The amplitude of each sideband oscillates with increasing $V_{\text{abs}}^{\text{PP}}$ according to J_l^2 (Supporting Fig. S4). This explains the overall shape of the structures in Fig. 2a which evolve from the non-linearities at $V = 2\Delta/ne$ associated with MAR. The highly asymmetric MAR features in Fig. 1e makes the inflection points of dV/dI – i.e. peaks in d^2V/dI^2 – well suited for identifying the onset of MAR as shown in Fig. 2b. The modulation period of the features associated with the $n = 1, 2, 3$ order MARs can be clearly resolved and as highlighted by the black arrows, the modulation period is not the same for each ‘V’-fan but rather decreases with decreasing bias. This is inconsistent with the conventional Tien-Gordon model described above which predicts the same characteristic pattern evolving from all non-linearities in I^0 . Instead, as discussed in the introduction, the pattern in Fig. 2a,b follows the work of Refs^{32,33} suggesting that Eq. 1 describes the microwave response for higher-order tunnel processes if the electron charge, e , is replaced by the total transferred charge $q = ne$: Refs^{32,33} experimentally confirmed this for quasiparticle (e) and incoherent Cooper pair tunneling at zero bias ($2e$). For our case, the n^{th} order MAR transfers ne electrons (Fig. 1f), and the corresponding modulation period should be $\Delta V_n = hf/ne$. For $f = 6$ GHz this amounts to $24.8 \mu\text{V}$, $12.4 \mu\text{V}$, and $8.3 \mu\text{V}$ for $n = 1, 2, 3$, respectively, in good agreement with the measured splittings $23.8 \mu\text{V}$, $12.2 \mu\text{V}$, and $9.3 \mu\text{V}$ from Fig. 2a,b (see below). Using this assumption we show in Fig. 2c the result of a simulation of d^2I/dV^2 taking the $I - V$ curve in absence of radiation as input and evolving according to Eq. 1 under the simplifying assumption that the n^{th} order MAR dominate in the region around $2\Delta/ne$ as shown by the dashed lines Fig. 2c (see Supporting Section IV for details). Comparing to Fig. 2b, the simulation accurately captures the main features of the measurement.

To further quantify the splitting, the measurements of Fig. 2a were repeated for different frequencies $f = 5 - 12$ GHz. Three representative examples are shown in Fig. 3a for $f = 6, 8, 10$ GHz. The coupling between the antenna and device depends strongly and non-monotonically on f , and therefore the amplitude of absorbed radiation, $V_{\text{abs}}^{\text{PP}}$ in Fig. 3a was

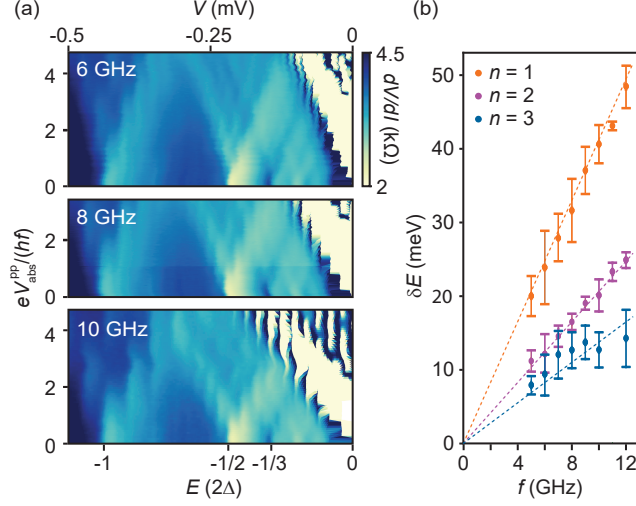


Figure 3: (a) dV/dI vs V and normalised absorbed microwave voltage $eV_{\text{abs}}^{\text{pp}}/(hf)$ for $f = 6, 8$ and 10 GHz. The 6 GHz data is a subset of Fig. 2a. The sideband spacing within each MAR order increases with increasing f . (b) Average sideband spacing $\langle \delta E \rangle$ as a function of f for $n = 1, 2, 3$ (blue, orange and green data points). The blue, orange and green dashed lines show the theoretical δE vs f relationships for 1, 2 and 3 electron processes.

for visualization purposes normalized to the first zero of J_0 which occurs at $eV_{\text{abs}}^{\text{pp}}/(hf) = 2.4$ (see Supporting information for non-normalized data at all eight frequencies). Figure 3b shows the average of the sideband spacing $\langle \delta E \rangle = e \langle \delta V \rangle$, as a function of f (data points) and the theoretical relationship $\delta E = hf/n$ (dashed lines) for $n = 1, 2$ and 3 (blue, orange and green). The average was obtained across all the measured δE within each order, and the error bars represent the standard deviation. The good agreement between theory and experiment quantitatively confirms that the n^{th} order MAR process involves the transmission of n electrons across the junction.

In conclusion, we have studied the finite-bias sub-gap structure in epitaxial InAsSb/Al JJs under microwave radiation. We showed that the microwave response provides a sensitive probe of the transmitted charge $q = ne$ up to order $n = 3$ – i.e. a MAR process including two Andreev reflections. The modulation period was found to decrease with increasing MAR order, and the dependence of the sideband spacings on the radiation amplitude agrees quantitatively with the expectation that each order transmits n electrons across the junction. A simulation based on a modified version of the Tien-Gordon equation was found to accu-

rately reproduce the measurements. We expect the effect to be observable in non-epitaxially matched hybrids, albeit likely with less sharp features than observed here,⁴² and possibly modified weight of the MAR due to changes in the interface transmission.¹⁶ We believe that the results will be valuable tool for understanding the low-energy sub-gap spectrum in hybrid nanoscale devices. This becomes increasingly relevant with the rapid developments in the quality of hybrid quantum materials, device fabrication and filtering and measurement techniques, which allows for increasing coherence lengths and increased spectral resolution and thus even higher order MAR at progressively lower energies. Finally, the identification of sub-gap states is a crucial task for the powerful technique of spatially resolved superconducting scanning tunneling microscopy.

Acknowledgement This research was supported by the Danish National Research Foundation, Microsoft Quantum Materials Lab, and by research grants from Villum Fonden (00013157), The Danish Council for Independent Research (7014-00132), and European Research Council (866158).

Competing interests

The authors declare no competing interests.

Supporting Information

The supporting information contains additional data relating to the excess current, Shapiro steps, PAT of MAR at a different gate voltage, the underlying measurements for Fig. 3, as well as extra information regarding the simulation in Fig. 2c. This material is available free of charge via the internet at <http://pubs.acs.org>.

References

- (1) Josephson, B. Possible new effects in superconductive tunnelling. *Phys. Lett.* **1962**, *1*, 251–253.
- (2) Kjaergaard, M.; Schwartz, M. E.; Braumüller, J.; Krantz, P.; Wang, J. I.-J.; Gustavsson, S.; Oliver, W. D. Superconducting Qubits: Current State of Play. *Annu. Rev. Condens. Matter Phys.* **2020**, *11*, 369–395.
- (3) Doh, Y.; van Dam, J.; Roest, A.; Bakkers, E.; Kouwenhoven, L.; De Franceschi, S. Tunable supercurrent through semiconductor nanowires. *Science* **2005**, *309*, 272–275.
- (4) Larsen, T. W.; Petersson, K. D.; Kuemmeth, F.; Jespersen, T. S.; Krogstrup, P.; Nygård, J.; Marcus, C. M. Semiconductor-Nanowire-Based Superconducting Qubit. *Phys. Rev. Lett.* **2015**, *115*, 127001.
- (5) Hays, M.; de Lange, G.; Serniak, K.; van Woerkom, D. J.; Bouman, D.; Krogstrup, P.; Nygård, J.; Geresdi, A.; Devoret, M. H. Direct Microwave Measurement of Andreev-Bound-State Dynamics in a Semiconductor-Nanowire Josephson Junction. *Phys. Rev. Lett.* **2018**, *121*, 047001.
- (6) Oreg, Y.; Refael, G.; von Oppen, F. Helical Liquids and Majorana Bound States in Quantum Wires. *Phys. Rev. Lett.* **2010**, *105*, 177002.
- (7) Lutchyn, R. M.; Sau, J. D.; Das Sarma, S. Majorana Fermions and a Topological Phase Transition in Semiconductor-Superconductor Heterostructures. *Phys. Rev. Lett.* **2010**, *105*, 077001.
- (8) Giaever, I. Energy Gap in Superconductors Measured by Electron Tunneling. *Phys. Rev. Lett.* **1960**, *5*, 147–148.
- (9) Deacon, R. S.; Tanaka, Y.; Oiwa, A.; Sakano, R.; Yoshida, K.; Shibata, K.; Hi-

- rakawa, K.; Tarucha, S. Tunneling Spectroscopy of Andreev Energy Levels in a Quantum Dot Coupled to a Superconductor. *Phys. Rev. Lett.* **2010**, *104*, 076805.
- (10) Pillet, J.-D.; Quay, C. H. L.; Morfin, P.; Bena, C.; Yeyati, A. L.; Joyez, P. Andreev Bound States in Supercurrent-Carrying Carbon Nanotubes Revealed. *Nature Phys* **2010**, *6*, 965–969.
- (11) Chauvin, M.; vom Stein, P.; Pothier, H.; Joyez, P.; Huber, M. E.; Esteve, D.; Urbina, C. Superconducting Atomic Contacts under Microwave Irradiation. *Phys. Rev. Lett.* **2006**, *97*, 067006.
- (12) Heedt, S. et al. Shadow-Wall Lithography of Ballistic Superconductor–Semiconductor Quantum Devices. *Nat. Commun.* **2021**, *12*, 4914.
- (13) Octavio, M.; Tinkham, M.; Blonder, G.; Klapwijk, T. Subharmonic energy-gap structure in superconducting constrictions. *Phys. Rev. B* **1983**, *27*, 6739–6746.
- (14) Blonder, G.; Tinkham, M.; Klapwijk, T. Transition from metallic to tunneling regimes in superconducting micro-constrictions - excess current, charge imbalance, and super-current conversion. *Phys. Rev. B* **1982**, *25*, 4515–4532.
- (15) Bratus, E.; Shumeiko, V.; Wendin, G. Theory of subharmonic gap structure in superconducting mesoscopic tunnel contacts. *Phys. Rev. Lett.* **1995**, *74*, 2110–2113.
- (16) Averin, D.; Bardas, A. ac Josephson Effect in a Single Quantum Channel. *Phys. Rev. Lett.* **1995**, *75*, 1831–1834.
- (17) Kjaergaard, M.; Suominen, H. J.; Nowak, M. P.; Akhmerov, A. R.; Shabani, J.; Palmstrøm, C. J.; Nichele, F.; Marcus, C. M. Transparent Semiconductor-Superconductor Interface and Induced Gap in an Epitaxial Heterostructure Josephson Junction. *Phys. Rev. Applied* **2017**, *7*, 034029.

- (18) Scheer, E.; Agrait, N.; Cuevas, J.; Yeyati, A.; Ludoph, B.; Martin-Rodero, A.; Bollinger, G.; van Ruitenbeek, J.; Urbina, C. The signature of chemical valence in the electrical conduction through a single-atom contact. *Nature* **1998**, *394*, 154–157.
- (19) Goffman, M. F.; Urbina, C.; Pothier, H.; Nygård, J.; Marcus, C. M.; Krogstrup, P. Conduction Channels of an InAs-Al Nanowire Josephson Weak Link. *New J. Phys.* **2017**, *19*, 092002.
- (20) Buitelaar, M.; Belzig, W.; Nussbaumer, T.; Babic, B.; Bruder, C.; Schönenberger, C. Multiple Andreev reflections in a carbon nanotube quantum dot. *Phys. Rev. Lett.* **2003**, *91*, 057005.
- (21) Eichler, A.; Weiss, M.; Oberholzer, S.; Schönenberger, C.; Levy Yeyati, A.; Cuevas, J. C.; Martin-Rodero, A. Even-odd effect in Andreev transport through a carbon nanotube quantum dot. *Phys. Rev. Lett.* **2007**, *99*, 126602.
- (22) Sand-Jespersen, T.; Paaske, J.; Andersen, B. M.; Grove-Rasmussen, K.; Jorgensen, H. I.; Aagesen, M.; Sorensen, C. B.; Lindelof, P. E.; Flensberg, K.; Nygård, J. Kondo-enhanced Andreev tunneling in InAs nanowire quantum dots. *Phys. Rev. Lett.* **2007**, *99*, 126603.
- (23) Dolcini, F.; Dell’Anna, L. Multiple Andreev Reflections in a Quantum Dot Coupled to Superconducting Leads: Effect of Spin-Orbit Coupling. *Phys. Rev. B* **2008**, *78*, 024518.
- (24) Hajer, J.; Kessel, M.; Brüne, C.; Stehno, M. P.; Buhmann, H.; Molenkamp, L. W. Proximity-Induced Superconductivity in CdTe–HgTe Core–Shell Nanowires. *Nano Lett.* **2019**, *19*, 4078–4082.
- (25) Abay, S.; Persson, D.; Nilsson, H.; Wu, F.; Xu, H. Q.; Fogelström, M.; Shumeiko, V.; Delsing, P. Charge transport in InAs nanowire Josephson junctions. *Phys. Rev. B* **2014**, *89*, 214508.

- (26) Xiang, J.; Vidan, A.; Tinkham, M.; Westervelt, R. M.; Lieber, C. M. Ge/Si nanowire mesoscopic Josephson junctions. *Nat. Nanotechnol.* **2006**, *1*, 208–213.
- (27) Peters, O.; Bogdanoff, N.; Acero González, S.; Melischek, L.; Simon, J. R.; Reece, G.; Winkelmann, C. B.; von Oppen, F.; Franke, K. J. Resonant Andreev Reflections Probed by Photon-Assisted Tunnelling at the Atomic Scale. *Nat. Phys.* **2020**, *16*, 1222–1226.
- (28) Cuevas, J.; Martin-Rodero, A.; Yeyati, A. Shot noise and coherent multiple charge transfer in superconducting quantum point contacts. *Phys. Rev. Lett.* **1999**, *82*, 4086–4089.
- (29) Cron, R.; Goffman, M.; Esteve, D.; Urbina, C. Multiple-charge-quanta shot noise in superconducting atomic contacts. *Phys. Rev. Lett.* **2001**, *86*, 4104–4107.
- (30) Kozhevnikov, A.; Schoelkopf, R.; Prober, D. Observation of photon-assisted noise in a diffusive normal metal-superconductor junction. *Phys. Rev. Lett.* **2000**, *84*, 3398–3401.
- (31) Ronen, Y.; Cohen, Y.; Kang, J.-H.; Haim, A.; Rieder, M.-T.; Heiblum, M.; Mahalu, D.; Shtrikman, H. Charge of a quasiparticle in a superconductor. *P. Natl. Acad. Sci.* **2016**, *113*, 1743–1748.
- (32) Kot, P.; Drost, R.; Uhl, M.; Ankerhold, J.; Cuevas, J. C.; Ast, C. R. Microwave-Assisted Tunneling and Interference Effects in Superconducting Junctions under Fast Driving Signals. *Phys. Rev. B* **2020**, *101*, 134507.
- (33) Roychowdhury, A.; Dreyer, M.; Anderson, J. R.; Lobb, C. J.; Wellstood, F. C. Microwave Photon-Assisted Incoherent Cooper-Pair Tunneling in a Josephson STM. *Phys. Rev. Applied* **2015**, *4*, 034011.
- (34) Tien, P.; Gordon, J. Multiphoton process observed in interaction of microwave fields with tunneling between superconductor films. *Phys. Rev.* **1963**, *129*, 647.

- (35) Platero, G.; Aguado, R. Photon-assisted transport in semiconductor nanostructures. *Phys. Rep.* **2004**, *395*, 1–157.
- (36) Khan, S. A. et al. Highly Transparent Gatable Superconducting Shadow Junctions. *ACS Nano* **2020**, *14*, 14605–14615.
- (37) Carrad, D. J.; Bjergfelt, M.; Kanne, T.; Aagesen, M.; Krizek, F.; Fiordaliso, E. M.; Johnson, E.; Nygård, J.; Jespersen, T. S. Shadow Epitaxy for In Situ Growth of Generic Semiconductor/Superconductor Hybrids. *Adv. Mater.* *32*, 1908411.
- (38) Gazibegovic, S. et al. Epitaxy of advanced nanowire quantum devices. *Nature* **2017**, *548*, 434.
- (39) Krizek, F.; Kanne, T.; Razmadze, D.; Johnson, E.; Nygård, J.; Marcus, C. M.; Krogstrup, P. Growth of InAs Wurtzite Nanocrosses from Hexagonal and Cubic Basis. *Nano Lett.* **2017**, *17*, 6090–6096.
- (40) Krogstrup, P.; Ziino, N. L. B.; Chang, W.; Albrecht, S. M.; Madsen, M. H.; Johnson, E.; Nygård, J.; Marcus, C. M.; Jespersen, T. S. Epitaxy of semiconductor-superconductor nanowires. *Nat. Mater.* **2015**, *14*, 400–406.
- (41) Sestoft, J. E.; Kanne, T.; Gejl, A. N.; von Soosten, M.; Yodh, J. S.; Sherman, D.; Tarasinski, B.; Wimmer, M.; Johnson, E.; Deng, M.; Nygård, J.; Jespersen, T. S.; Marcus, C. M.; Krogstrup, P. Engineering Hybrid Epitaxial InAsSb/Al Nanowires for Stronger Topological Protection. *Phys. Rev. Materials* **2018**, *2*, 044202.
- (42) Chang, W.; Albrecht, S. M.; Jespersen, T. S.; Kuemmeth, F.; Krogstrup, P.; Nygård, J.; Marcus, C. M. Hard gap in epitaxial semiconductor–superconductor nanowires. *Nat. Nanotechnol.* **2015**, *10*, 232–236.
- (43) McCumber, D. E. Effect of ac Impedance on dc Voltage-Current Characteristics of Superconductor Weak-Link Junctions. *Journal of Applied Physics* **1968**, *39*, 3113–3118.

- (44) Tinkham, M.; Free, J. U.; Lau, C. N.; Markovic, N. Hysteretic I-V curves of superconducting nanowires. *Phys. Rev. B* **2003**, *68*, 134515.
- (45) Flensberg, K.; Hansen, J. B.; Octavio, M. Subharmonic energy-gap structure in superconducting weak links. *Phys. Rev. B* **1988**, *38*, 8707–8711.
- (46) Deng, M. T.; Vaitiekėnas, S.; Hansen, E. B.; Danon, J.; Leijnse, M.; Flensberg, K.; Nygård, J.; Krogstrup, P.; Marcus, C. M. Majorana bound state in a coupled quantum-dot hybrid-nanowire system. *Science* **2016**, *354*, 1557–1562.
- (47) Klapwijk, T.; Blonder, G.; Tinkham, M. Explanation of subharmonic energy gap structure in superconducting contacts. *Physica B+C* **1982**, *109-110*, 1657–1664, 16th International Conference on Low Temperature Physics, Part 3.
- (48) Ridderbos, J.; Brauns, M.; Li, A.; Bakkers, E. P. A. M.; Brinkman, A.; van der Wiel, W. G.; Zwanenburg, F. A. Multiple Andreev reflections and Shapiro steps in a Ge-Si nanowire Josephson junction. *Phys. Rev. Materials* **2019**, *3*, 084803.
- (49) Shapiro, S. Josephson Currents in Superconducting Tunneling: The Effect of Microwaves and Other Observations. *Phys. Rev. Lett.* **1963**, *11*, 80–82.
- (50) Larson, T. F. Q.; Zhao, L.; Arnault, E. G.; Wei, M.-T.; Seredinski, A.; Li, H.; Watanabe, K.; Taniguchi, T.; Amet, F.; Finkelstein, G. Zero Crossing Steps and Anomalous Shapiro Maps in Graphene Josephson Junctions. *Nano Letters* **2020**, *20*, 6998–7003.
- (51) Perla, P.; Fonseca, H. A.; Zellekens, P.; Deacon, R.; Han, Y.; Kölzer, J.; Mörstedt, T.; Bennemann, B.; Espiari, A.; Ishibashi, K.; Grützmacher, D.; Sanchez, A. M.; Lepsa, M. I.; Schäpers, T. Fully *in Situ* Nb/InAs-nanowire Josephson Junctions by Selective-Area Growth and Shadow Evaporation. *Nanoscale Adv.* **2021**, *3*, 1413–1421.